Article:
Califano, M orcid.org/0000-0003-3199-3896, Lu, R and Zhou, Y (2021) Indirect to Direct Band Gap Transformation by Surface Engineering in Semiconductor Nanostructures. ACS Nano, 15 (12). pp. 20181-20191. ISSN 1936-0851

https://doi.org/10.1021/acsnano.1c08176

Indirect to Direct Band Gap Transformation by Surface Engineering in Semiconductor Nanostructures

Marco Califano,*,†,‡ Ruiyan Lu,¶ and Yeke Zhou¶

† *Pollard Institute, School of Electronic and Electrical Engineering, University of Leeds, Leeds LS2 9JT, United Kingdom*

‡ *Bragg Centre for Materials Research University of Leeds, Leeds LS2 9JT, United Kingdom*

¶ *School of Electronic and Electrical Engineering, University of Leeds, Leeds LS2 9JT, United Kingdom*

E-mail: m.califano@leeds.ac.uk

Abstract

Indirect band gap semiconductor materials are routinely exploited in photonics, optoelectronics and energy harvesting. However, their optical conversion efficiency is low, due to their poor optical properties, and a wide range of strategies, generally involving doping or alloying, has been explored to increase it, often, however, at the cost of changing their material properties and their band gap energy, which, in essence, amounts to changing them into different materials altogether. A key challenge is therefore to identify effective strategies to substantially enhance optical transitions at the band gap in these materials, without sacrificing their intrinsic nature. Here we show that this is indeed possible, and that GaP can be transformed into a direct gap material by simple nanostructuring and surface engineering, while fully preserving its "identity". We then distill the main ingredients of this procedure into

a general recipe applicable to any indirect material and test it on AlAs, obtaining an increase of over 4 orders of magnitude in both emission intensity and radiative rates.

Keywords

nanocrystals, indirect materials, GaP, AlAs, pseudopotential method, k-vector analysis, indirect-to-direct transitions

Introduction

Bulk GaP is characterized by a conduction band minimum (CBM) occurring at the six equivalent Δ-valleys, situated along the [100] directions toward the X-point of the Brillouin zone boundary, and by a valence band maximum (VBM) located at the Γ-point. This makes the fundamental band gap transition indirect and the zero-phonon transitions dipole forbidden. Despite this, GaP has been widely exploited as a photonic material for the past half a century in a range of light-emitting devices, and, in particular, in the production of green LEDs.[1]

However, owing to the indirect character of the material in its pure state, its measured conversion efficiency is low (about 0.1%).[2] Strategies to increase it have included the use of dopants (nitrogen, zinc or oxygen),[3,4] which, by introducing suitable recombination states in the band gap,[3] can lead to over 100-fold efficiency improvements. However, even in doped GaP green LEDs, the efficiency does not exceed a few percent.[2] Alternatively, larger improvements can be achieved by epitaxial growth of a direct gap ternary $GaAs_{1-y}P_y$ layer[5] as the active part of the LED. Indeed, alloying of GaP with different N,[6] In[7] and Sb[8] compositions has been shown to lead to a direct gap material, albeit with a reduced band gap.

GaP, being nearly lattice-matched to silicon, is also an excellent candidate to be part of a high band gap solar cell in a multi-junction system.[9,10] Furthermore, GaP films have

been utilized for photoelectrochemical reduction of CO_2 to methanol,[11] and in photocatalytic structures for water-splitting, where, however, low currents were reported[12] as a direct consequence of the indirect bandgap of GaP leading to poor light absorption.

A key challenge in GaP-based optoelectronics and photonics (and, in general, for any indirect material energy conversion application) is therefore to identify strategies to achieve stronger optical transitions at the bandgap. Here we show that this is indeed possible and, furthermore, that an indirect-to-direct band gap transition can be achieved in zincblende GaP nanostructures of suitable sizes by careful surface engineering. Based on these results, we then propose a simple general strategy, to transform any indirect band gap material into a direct one, and we validate it by successfully applying it to AlAs.

Results and Discussion

Over 25 years ago, theoretical band structure calculations[13,14] predicted a pseudo-direct nature of the band gap in *wurtzite* GaP, where the CBM is expected to occur at $k = 0$ (*i.e.*, at the Γ point), but to have Γ_8 symmetry (in double group notation) instead of Γ_7, as in the case of direct band gap semiconductors. It follows that, although CBM and VBM wave functions overlap in k-space, the optical transitions between these two states are impaired because of symmetry (hence the term *pseudo*-direct). This prediction was recently tested by Assali *et al.*[15] in vapor-liquid-solid-(VLS)-grown GaP nanowires (NWs) with pure hexagonal crystal structure, whose optical properties evidenced one order of magnitude increase in the integrated photoluminescence (PL) emission and about 2 orders of magnitude decrease in the PL lifetime when compared with those of a zincblende (001) bulk GaP reference sample. These features were attributed to the presence of a direct band gap in wurtzite NWs.

Strain,[16] alloying[17] and excitonic effects[18] were then predicted to further enhance the optical oscillator strength in GaP NWs. The presence of uniaxial tensile strain along the

c axis in wurtzite GaP NWs was predicted[16] to lead to a crossover between Γ_{7c} (which red-shifts with increasing strain) and Γ_{8c} (which blue-shifts under the same conditions), hence to a pseudo-direct-to-direct transition in these systems. However, the excitonic-like emission observed in GaP NWs was attributed[16] to transitions involving localised states (deep centres), whose symmetry included a significant contribution from Γ_{7c}, owing to the limited spatial extent (and corresponding large delocalisation in k-space) of the impurities.

As the lowest conduction band in wurtzite InP has Γ_{7c} symmetry, whereas that of wurtzite GaP Γ_{8c} symmetry, it is expected that the CBM in $In_xGa_{1-x}P$ should exhibit a crossover between Γ_{8c} and Γ_{7c} for some value of x. This effect has been recently observed[17] in GaP/$In_xGa_{1-x}P$ core/shell NWs.

The observation of strong, although theoretically nearly dipole-forbidden, Γ_{8c} to Γ_{9v} transitions in GaP NWs has been rationalised theoretically[18] by invoking a delocalization of the exciton envelope function in k-space due to its finite extent (of the order of the exciton radius, estimated at 2.5-3.2 nm) in real space. However, alternative sources were also suggested for such an oscillator strength enhancement, including defects, internal electric fields, and band bending.[18]

Recently, Kim *et al.*[19] reported luminescence from the direct band gap transitions in GaP nanocrystals (NCs) synthesized *via* a hot-injection method, attributing it to a confinement-induced '*expansion of the band edge wave functions in momentum space*',[19] which enabled emission at wavelengths close to those of the indirect transition in the bulk. However some of the reported emission features (double-peaked PL spectrum and multi-exponential decay with lifetimes of the order of 1 ns) are strikingly similar to those reported by Furis *et al.*[20] and attributed to the surfactants commonly utilized to arrest growth and/or agglomerization in the synthesis of GaP nanoparticles (rather than to emission from the nanoparticles themselves), which have been found to exhibit optical properties similar to those observed for nanocrystals with broad size distributions.

Therefore the origin of the strong band edge emission observed in GaP NCs by Kim *et al.*[19] remains controversial.

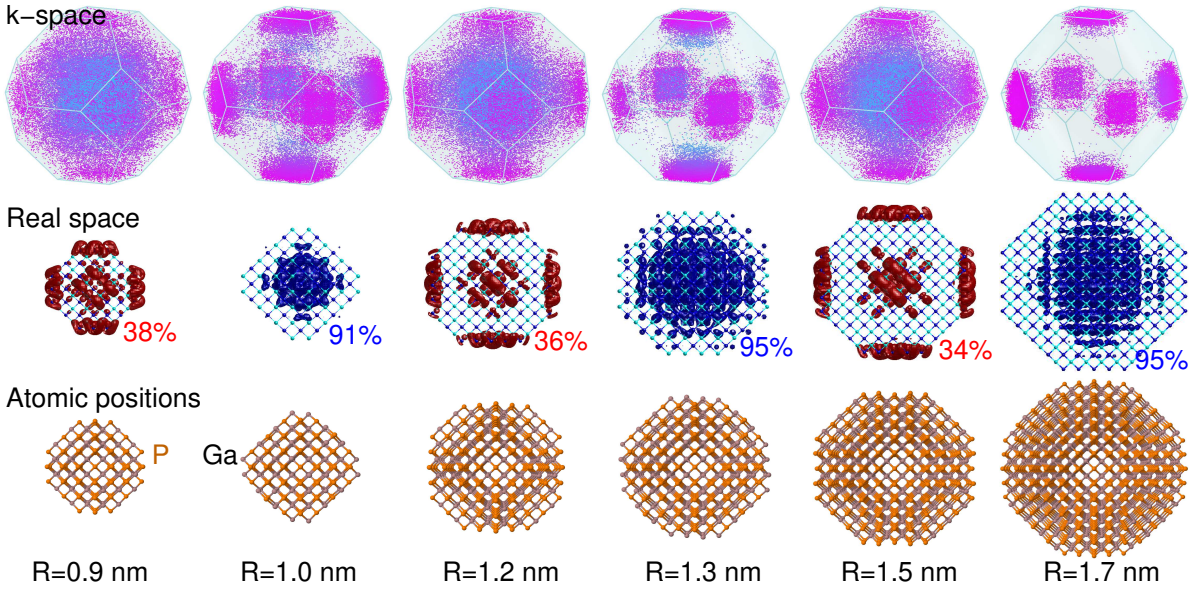

Figure 1: Upper row: 3D representation of the first Brillouin zone showing the reciprocal space composition of the CBM wave function (k-points close to Γ are shown in blue, and k-points close to L and X are colored in magenta); middle row: corresponding 3D charge densities in real space (the value of the electron density calculated within a sphere with $R_{sphere} = 0.9R_{NC}$, concentric with the NC, is also shown); bottom row: the atomistic structure of the NCs (orange spheres represent P atoms and grey spheres Ga atoms), evidencing that NCs with $R = 0.9$, 1.2, 1.5 and 1.7 nm display P-rich facets along the (100), (010), and (001) (and equivalent) directions, whereas NCs with $R = 1$ and 1.3 nm have Ga-rich facets along those directions (Further details about the surface composition of these GaP NCs are provided in Fig. S1, Supporting Information).

In order to shed light on this issue, we applied our state-of-the-art atomistic semiempirical pseudopotential method[21] to investigate the properties of GaP nanocrystals with sizes ranging from 0.9 nm to 3.5 nm. In contrast to Kim *et al.*,[19] we find that confinement alone is not sufficient to yield a direct band gap transition in GaP NCs, even for sizes as small as $R \sim 1$ nm. However, if size reduction is combined with the presence of P-rich surfaces, the resulting CBM wave function exhibits a prevalent Γ character. This effect is clearly visible in the upper panels of Fig. 1, where we display the CBM wave function calculated for six NC sizes (with 0.9 nm $\leq R \leq$ 1.7 nm), with different surface stoichiometries, both in k-space (upper row - represented in the 3D first Brillouin zone,

where k-points close to Γ are shown in blue, and k-points close to L and X are colored in magenta), and in real space (middle row - where the value of the electron density calculated within a sphere with $R_{sphere} = 0.9R_{NC}$, concentric with the NC, is also shown), together with the atomistic NC structure (lower row - where orange spheres represent P atoms and grey spheres Ga atoms): NCs with $R = 0.9$, 1.2, 1.5 and 1.7 nm display P-rich facets along the (100), (010), and (001) (and equivalent) directions, whereas NCs with $R = 1$ and 1.3 nm have Ga-rich facets along those directions (further details about the surface composition of the GaP NCs considered here can be found in Fig. S1, Supporting Information). The CBM wave functions of the latter are well localised within the NC (with over 90% of the electron charge contained within 90% of the NC radius), and have mainly X character in k-space. In contrast, NCs with $R = 0.9$, 1.2 and 1.5 nm exhibit a CBM wave function that is mostly localised on the surface (only less than 40% of the electron charge is within 90% of the NC radius), and has strong Γ character. Interestingly, the CBM wave function of NCs with $R \geq 1.7$ nm exhibits the same characteristics as those with Ga-rich surfaces, despite having a P-rich surface, suggesting that confinement plays, indeed, an important role.

The energies of the lowermost X-like and Γ-like conduction band states (calculated with respect to the vacuum level) are plotted in Fig. 2 for different sizes. We note the following: (i) dots with Ga-rich surfaces exhibit a 3-fold degenerate (excluding spin) X-like CBM (black solid circles), with the singly degenerate Γ-derived state (black open circles) located at a very high energy above it; (ii) dots with P-rich surfaces have a singly degenerate, mainly Γ-like CBM (red solid circles), followed by a 3-fold degenerate X-like state (red open circles) that, however, becomes the CBM for $R = 1.7$ nm (red nearly solid circle); (iii) dots with $R > 1.7$ nm exhibit a 3-fold degenerate X-like CBM, irrespective of their surface stoichiometry, with the singly degenerate Γ-derived state located at a much higher energy. We conclude that the strong mixing of Γ character into the CBM is due to a combination of confinement and surface termination. The difference between the wave

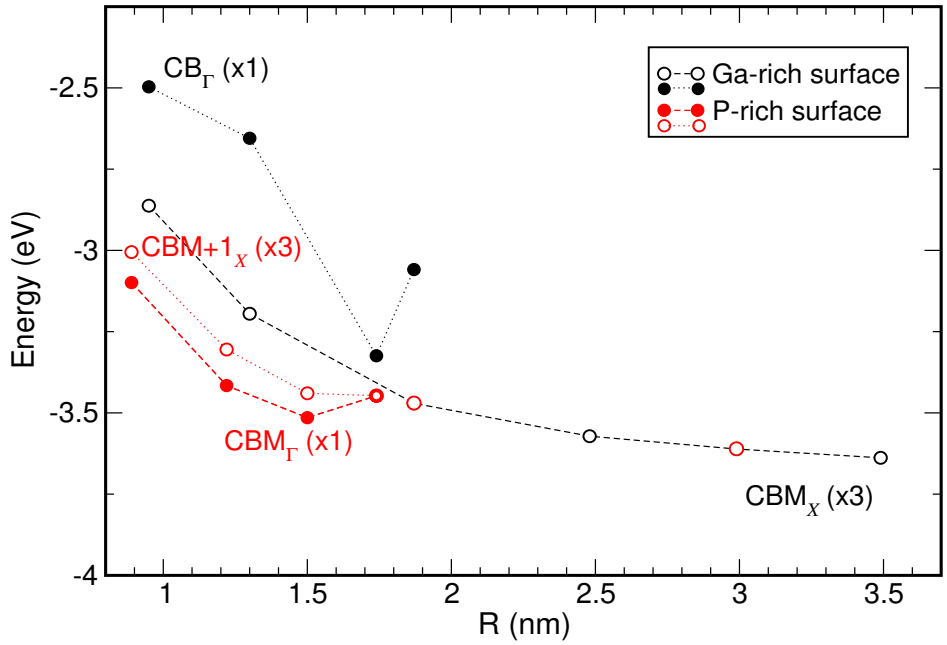

Figure 2: The energies of the lowermost X-like (empty circles) and Γ-like (solid circles) conduction band states (calculated with respect to the vacuum level) in GaP NCs with Ga-rich surfaces (black circles) and P-rich surfaces (red circles). The lines are a guide to the eye. The degeneracy of the states ($\times$ n, without accounting for spin), is also displayed.

function character in NCs with different surface stoichiometries is further highlighted in Fig. 3, where we show the contribution from the bulk Bloch functions from different high-symmetry points (HSPs) to all conduction band states within 3.6 eV from the VBM: whilst Ga-rich surfaces lead to strong X character for most of the electronic states (that approaches 100% for states close to the band edge), the presence of P atoms on the surface promotes stronger inter-valley mixing, resulting in higher Γ and L character in all CB states.

Such a larger mixing of direct Γ-like wave function character into the indirect X-like conduction band states leads to an enhancement of the zero-phonon transitions. This is evident from the comparison between the optical spectra calculated for these two types of NCs, presented in Fig. 4 (where the red curves denote absorption and the blue emission). In NCs with Ga-rich surfaces (*e.g.*, $R = 1.3$ nm) the absorption exhibits a shoulder (at around 350-360 nm, in Fig. 4a), followed by a long tail (that extends to about 430 nm

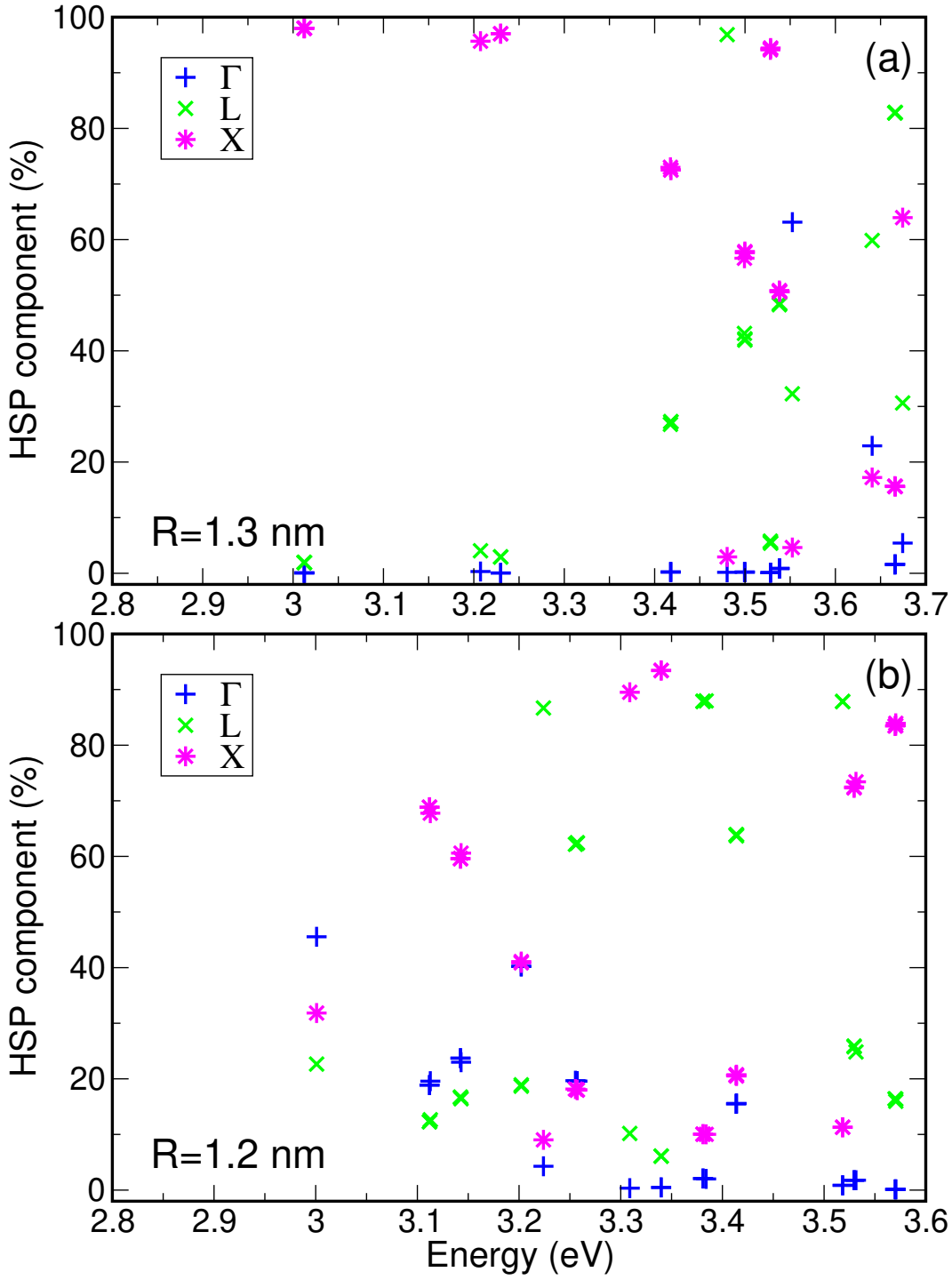

Figure 3: Fraction of high symmetry points (HSP)-component of bulk Bloch functions in each conduction band state, for GaP NCs with radii 1.3 (a) and 1.2 nm (b): Γ, blue plusses (+); X, magenta stars (*); L, green crosses (x). Each vertical set of (+,*,x) symbols corresponds to a single electronic state, whose energy is calculated from the VBM.

in Fig. 4a), as observed experimentally,[19,22,23] and commonly attributed to direct (Γ_V to Γ_C) and indirect (Γ_V to X_C) transitions, respectively.[19,22,23] The emission is much weaker (its amplitude is multiplied by 5×10^4 in Fig. 4a), and located at a much lower energy, compared to the position of the absorption shoulder, evidencing a huge Stokes shift (here of the order of 650 meV), also in agreement with experimental observation.

In contrast, in NCs with P-rich surfaces (*e.g.*, $R = 1.2$ nm) the transitions responsible for absorption edge and emission (numbered arrows in the inset of Fig. 4b, corresponding to the peaks labelled in black as 1 to 3 in the main figure) coincide, yielding a negligible Stokes shift (which is non-zero only due to the weight of higher energy transitions, which cause a broadening and a slight blue shift of the first absorption peak). Furthermore, the emission intensity (whose amplitude is multiplied by 50 in Fig. 4b) is about 3 orders of magnitude stronger than in NCs with Ga-terminated facets, owing to the prevalent Γ-like nature of the CBM (see Fig. 1).

In both types of NCs, each peak in both the emission and the absorption spectrum can be decomposed into several smaller peaks (denoted in the figure by numbers, increasing with the peak's position in energy), each of which, in turn, is contributed to by many different transitions (identified by numbered arrows in the insets of Fig. 4, for the case of the emission - A detailed description of the origin of these peaks is provided in the Supporting Information).

The differences we find in the optical spectra of NCs with Ga-rich and P-rich surfaces are the consequence of the different values of the oscillator strength for transitions between band edge states in the two systems, and therefore reflect themselves in their radiative lifetimes too (see Fig. 5). The presence of a large Γ component in the CBM, leads to lifetimes of the order of hundreds of ns in NCs with P-rich surfaces. In contrast, NCs with Ga-rich surfaces exhibit CBM with nearly 100% X character, and radiative lifetimes ranging from tens of microseconds to milliseconds. Interestingly, however, when the NC radius exceeds ~ 1.6 nm, weak, indirect band edge transitions and long lifetimes (> 0.1

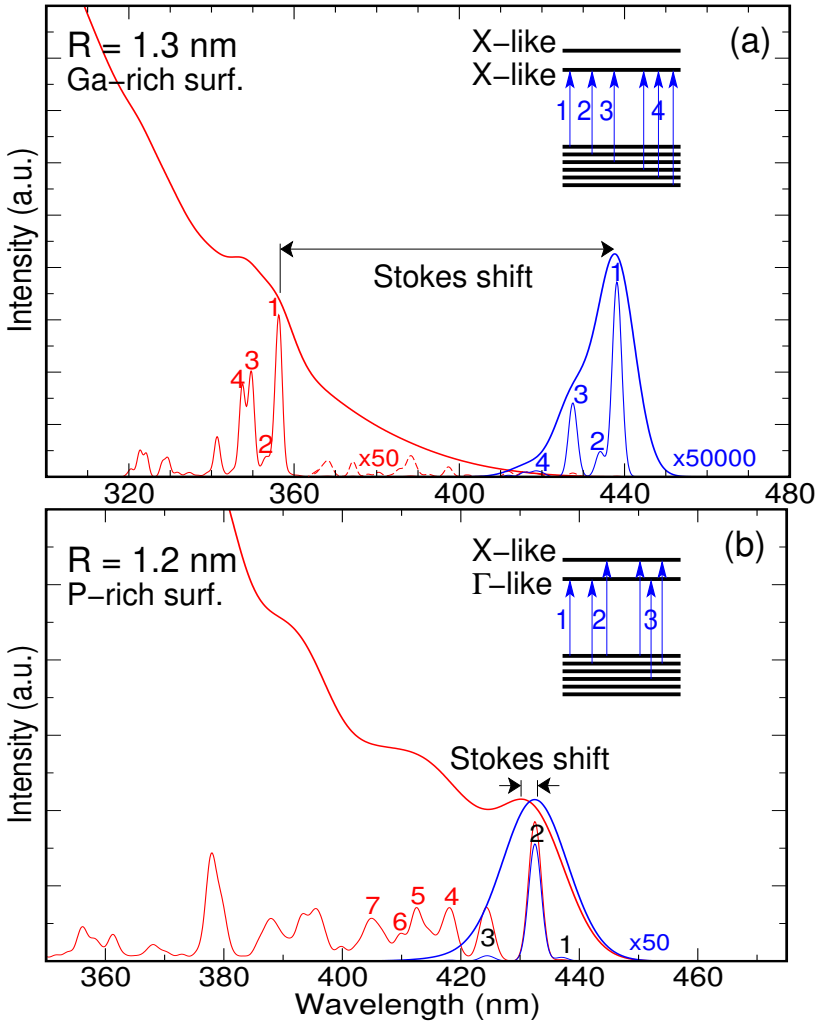

Figure 4: Optical spectra (PL: blue curves; absorption: red curves) calculated for GaP NCs with $R = 1.3$ nm and Ga-rich surfaces (a), and $R = 1.2$ nm and P-rich surfaces (b). The insets identify the transitions responsible for the different PL peaks and the prevalent character of the lowermost CB states. The blue curves are normalized to the absorption edge in (b) and to the shoulder in (a): the normalization constant is 5×10^4 in (a) and 50 in (b).

ms) are found for all surface terminations (see Fig. 5).

A similar size-dependent behaviour was also found in recent *ab initio* calculations,[24] which, however predicted a Γ_5-to-Γ_1 crossover in the nature of the CBM, leading to an enhancement of the band edge absorption, only in GaP nanocrystals with radii smaller than 0.75 nm, *i.e.*, outside the experimental range ($R \gtrsim 1$ nm).[19,22,23] Interestingly, the structure exhibiting such a crossover had a P-rich surface, as we find in our case. The different estimate for the crossover-size may derive from the reduced electronegativity of the pseudo-hydrogen atoms (*i.e.*, H with a modified nuclear charge of 0.75) used to passivate the NC surface anions in [24], which would require a stronger confinement to induce a perturbation sufficiently strong to promote character mixing in the CBM (see below).

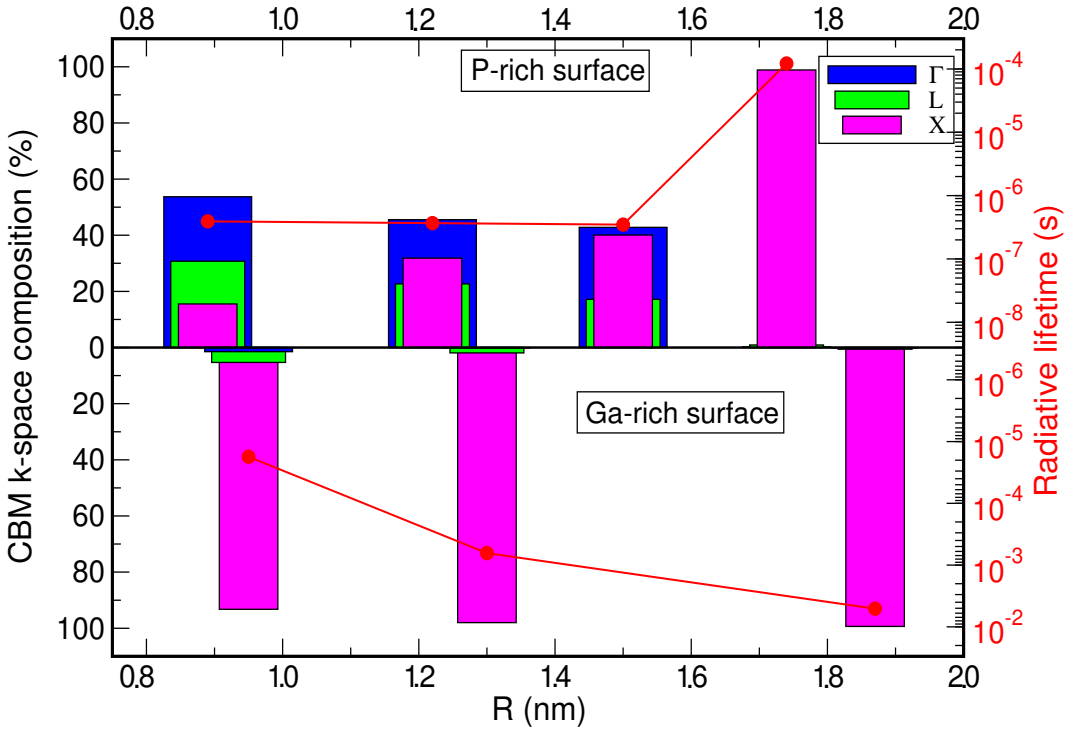

Figure 5: CBM k-space composition (Γ: blue bars; L: green bars; X: magenta bars) - left y axis - and radiative lifetimes (right y axis) calculated for GaP NCs with radii ranging from 0.9 to 1.9 nm.

The 3 orders of magnitude increase in the PL intensity and the 2 to 4 orders of magnitude decrease in the radiative lifetimes we find in GaP NCs with P-rich surfaces are in

striking contrast with the one order of magnitude increase in the integrated PL emission and about 2 orders of magnitude decrease in the PL lifetime observed in wurtzite GaP nanowires[15] (compared with those of a zincblende (001) bulk GaP reference sample), and adduced as evidence of a direct band gap in those nanostructures.

We will now discuss the possible origins of the enhanced optical transitions we found in small P-terminated GaP NCs. Our results identified two essential ingredients: (i) size and (ii) surface stoichiometry. (i) The forbidden nature of the band gap transitions in bulk GaP stems from momentum conservation laws. These are partially relaxed in NCs due to confinement. This effect is attributed[25] to Heisenberg's uncertainty principle, whereby strong spatial localization (Δr) in a NC results in a large momentum uncertainty (Δk), which spreads the wave functions in k-space to an extent inversely proportional to the NC size, allowing band edge optical transitions. As our results for Ga-terminated NCs have shown, however, confinement alone is not sufficient to promote a direct band gap transition in GaP NCs. Further spread of the band edges wave functions in reciprocal space necessitates the presence of an additional perturbation[26] which can promote stronger intervalley mixing and build a larger Γ component in the CBM. Such perturbation(s) can be of a structural (interfaces or surfaces, alloying, strain, shape asymmetries) or chemical (electronegativity of the ligands, polarity of the solvent, charges in the environment) nature. In our case, we attribute this effect to a surface scattering mechanism (originally proposed by Lee *et al.*[26] in Si NCs), enhanced here by (ii) the presence of P-terminated facets, which leads to an enhanced Γ-X mixing whose magnitude is inversely proportional to the energy separation between the X-like and Γ-like conduction band states close to the band edge. We find that the presence of P-terminated facets delocalises the electron wave function away from the NC core and close to the surface (see Fig. 1). As the effective mass at the Γ point is much smaller than that at X, such a deconfinement leads to a faster drop of the energy of Γ-like states, compared to that of X-like states, resulting in a reduction of their separation, compared to both the bulk and Ga-terminated NCs (see Fig. 2). This yields a

Γ-X mixing substantially stronger than that exhibited by the latter nanostructures, resulting in a Γ-like CBM. The fact that this effect is linked to the delocalisation of the electronic wave function towards the surface, suggests that an indirect-to-direct transition could also be induced by the presence of strongly electronegative ligands in GaP NCs with any surface stoichiometry. Most importantly, considering that in nearly all indirect semiconductors the effective mass at Γ is smaller than that at the CBM (located at X or L), a general strategy to enhance the zero-phonon transitions, or even to promote an indirect-to-direct transition, could be to use electronegative ligands to passivate the surface of NCs made of these materials.

We tested this hypothesis on GaP NCs first, over a wide range of experimentally relevant sizes, starting from $R = 1.7$ nm (*i.e.*, the smallest size with a P-rich surface for which the CBM's Γ component is negligible - see Fig. 1), which contains nearly 1100 atoms and exhibits strong faceting, and culminating with the quasi-spherical $R = 4.2$ nm, containing over 15000 atoms. From Fig. 6a, it is evident that, with an ideal passivation (ip), the CBM wave functions of all sizes are well confined to the dot core (dark blue regions in the 3D representation of the NCs in real space, pictured in the inset), and exhibit nearly 100% X character (magenta stars in the main panel and magenta dots in the 3D Brillouin zone representation in the inset). As a consequence, the PL is weak and the radiative lifetimes are long (see Fig. 6c and d). A slight increase in the electronegativity of the surface anion passivant (for details see Table S1, Supporting Information) led to a dramatic change in the CBM wave function localisation (that shifted from the core to the surface, see inset of Fig. 6b) and to the desired strong Γ-X mixing into its character (Fig. 6b). This resulted in greatly enhanced zero-phonon transitions and in an increase in PL intensity of up to over 4 orders of magnitude, with similar increases in the radiative rates (Fig. 6c and d).

In order to test the generality of this strategy, beyond GaP, we applied it to an indirect band gap material with a completely different composition: AlAs. Bulk AlAs has a band structure similar to that of GaP, with the minima of the CB near the X points of the

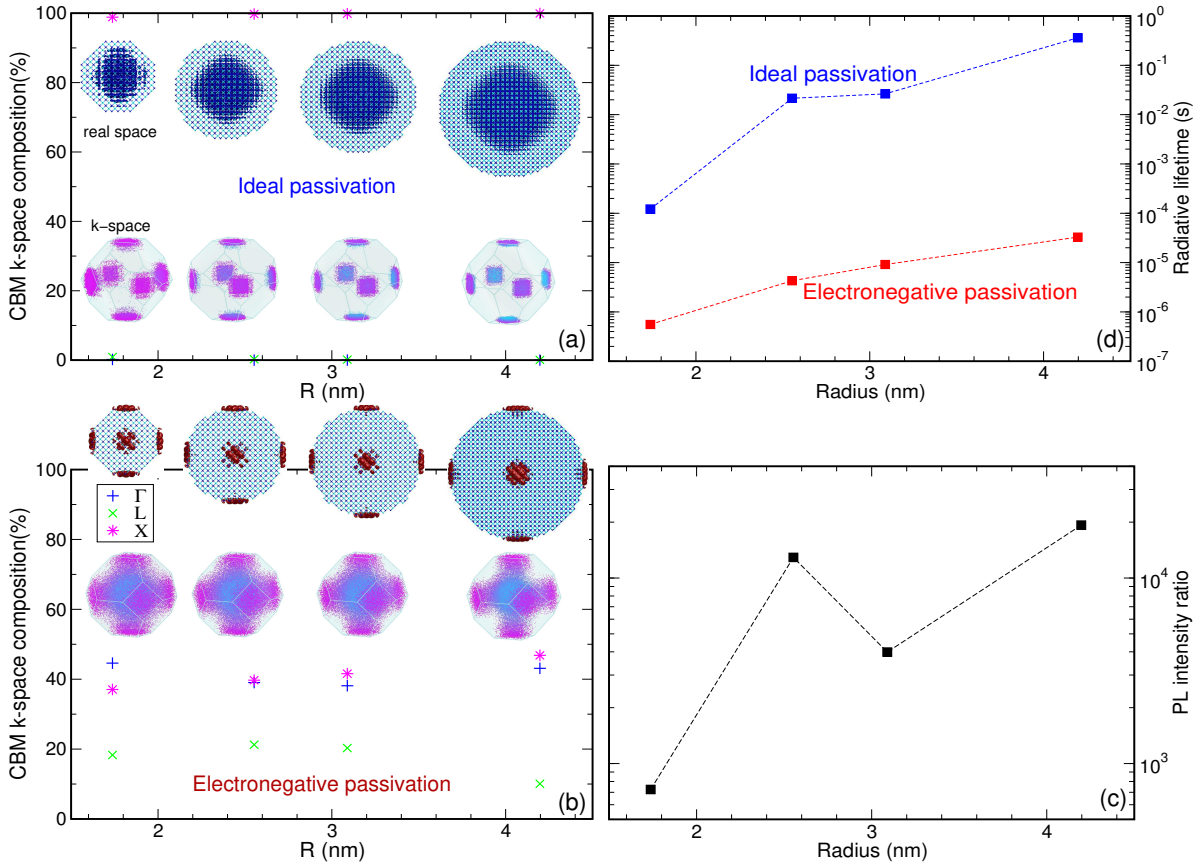

Figure 6: CBM k-space composition [(a) and (b)] calculated for GaP NCs with different sizes [Γ, blue plusses (+); X, magenta stars (*); L, green crosses (x). Each vertical set of (+,*,x) symbols corresponds to a single electronic state], and either (a) ideal passivation or (b) electronegative passivation. The insets in (a) and (b) represent the CBM wave function in k-space and real space (in the former, blue dots indicate k-points close to the Γ point, whereas magenta dots indicate k-points close to X and L; in the latter, blue and cyan spheres represent P and Ga atoms, respectively). (c) Ratio between the PL intensity of electronegatively passivated and ideally passivated GaP NCs *vs* size. (d) Radiative lifetimes *vs* size [ideal passivation, blue symbols and line; electronegative passivation, red symbols and line].

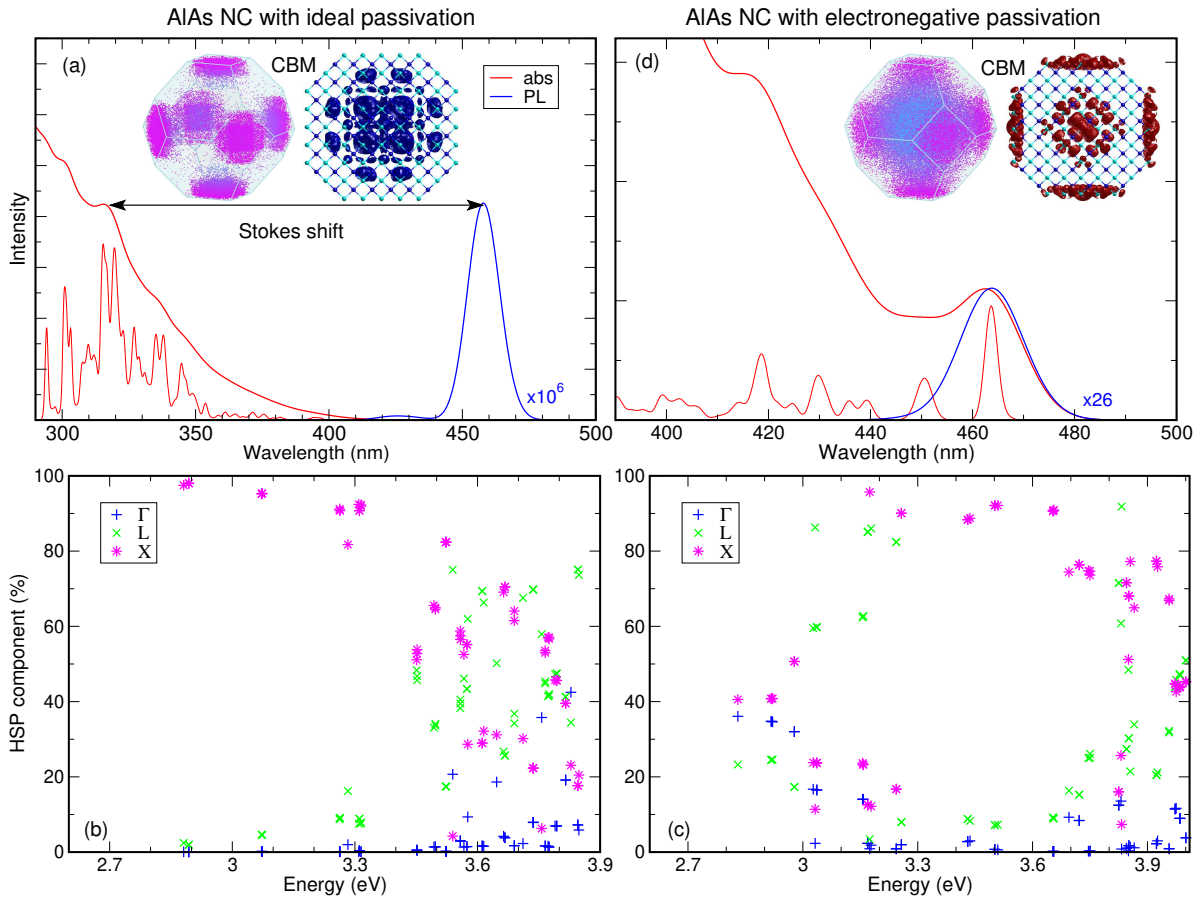

Figure 7: Optical spectra [(a) and (d); absorption, red line; emission, blue line] and high symmetry points (HSP) composition [(b) and (c)] of the 60 lowermost conduction band states [Γ, blue plusses (+); X, magenta stars (*); L, green crosses (x). Each vertical set of (+,*,x) symbols corresponds to a single electronic state, whose energy is calculated from the VBM], calculated for AlAs NCs with $R = 1.26$ nm and either (b) ideal passivation or (c) electronegative passivation. The insets in (a) and (d) represent the CBM wave function in k-space and real space (in the former, blue dots indicate k-points close to the Γ point, whereas magenta dots indicate k-points close to X and L; in the latter, blue and cyan spheres represent Al and As atoms, respectively).

Brillouin zone,[27] but a much larger energy difference ($\sim$ 0.9 eV) between the indirect gap (2.15 eV) and the direct gap (3.03 eV - both values measured at room temperature[27]). Furthermore, its effective masses at Γ and X (0.15 and 0.8,[28] respectively) satisfy the criterion above.

We started with a NC with $R = 1.26$ nm, similar in size to those considered in Fig. 3 and Fig.4. We first ran a set of calculations with a standard passivation, which yielded the expected results for a conventional indirect band gap material: (i) an X-like CBM, which exhibited almost 100% X character and nearly zero L and Γ components, and (ii) whose wave function in real space was well confined to the NC core (see insets in Fig. 7a); (iii) large X component and very low Γ component for most of the lowermost CB states (Fig. 7b); (iv) an absorption spectrum characterized by a main shoulder (located at 310-320 nm in Fig. 7a, and decomposed into unlabelled peaks - thin red lines) contributed to by a very large number of transitions, the strongest of which involve the CB states with high Γ component (and, in particular, the Γ-like state, which, for this specific dot size, is state $|e_{57}\rangle$), and a long tail (that extends to about 410 nm in Fig. 7a), that only involves transitions to X-like states. (v) a huge Stokes shift of over 1.2 eV, between an extremely weak emission (the blue curve is magnified by a factor of 10^6 in Fig. 7a), and the direct peak in absorption (red curve); (vi) a radiative lifetime of 10 ms. All these characteristics are reminiscent of those found in GaP NCs with a Ga-rich surface, such as $R = 1.3$ nm in Fig. 3a and Fig. 4a. These results clearly show that confinement alone is not sufficient to promote an indirect-to-direct transition or to even enhance optical transitions at the band edge in an indirect material. In order for this to be achieved, confinement needs to be combined with the presence of strongly electronegative ligands. Indeed, an increase in the electronegativity of the capping group passivating the surface anion promoted a strong inter-valley mixing in the CB states close to the band edge (Fig. 7c), resulting in enough Γ character to be mixed in an otherwise nearly 100% X-like CBM (compare Fig. 7b and Fig. 7c), to strongly enhance all zero-phonon transitions, and increase both the pho-

toluminescence intensity (Fig. 7d) and the radiative recombination rate by over 4 orders of magnitude.

We then repeated this procedure for a wide range of radii, finding that, like in the case of electronegatively passivated GaP NCs (Fig 6b), the CBM of AlAs NCs with an electronegative passivation exhibits a large Γ component (Fig. 8b) up to the largest size we considered - $R = 4.1$ nm, containing over 12500 atoms - (whereas the CBM and the lowermost 60 CB states of an ideally passivated dot of that size are nearly 100% X-like, as shown in Fig. 8a). As a consequence, the zero-phonon transition enhancement and the increase in PL intensity and radiative rates are preserved in large sizes of this material as well (see Fig. 8c and d).

Having shown that the mechanism we identified for promoting a strong inter-valley mixing in the CBM, leading to strongly enhanced optical transitions at the band edge (*i.e.*, to what can be defined as an indirect-to-direct transition), worked in two very different III-V materials, we wondered whether this strategy could be applicable to *any* indirect semiconductor. That this may indeed be the case is suggested by the ample theoretical and experimental evidence available in the case of Si NCs, where: (a) the presence of electronegative F passivation was shown, by DFT calculations,[29] to lead to an increase in both IE and in the delocalisation of the LUMO towards the surface, with increasing F coverage, resulting in an enhancement of up to a factor of 200 in the radiative recombination rates, in Si NCs with $D = 1.4$ nm; (b) Cl-capping in Si NCs resulted in bright white light emission;[30] (c) N-passivated Si nanoclusters were shown, by density functional tight-binding calculations,[31] to exhibit a LUMO localised close to the surface (in contrast to H-passivated ones, where the LUMO was delocalised throughout the cluster core), leading to significantly enhanced emission; (d) a quantum yield enhancement up to 75% was reported in oxidized Si NCs functionalised with N-containing aromatic species; (e) the fast radiative rates and strong emission observed in C-terminated Si NCs,[32] attributed to phonon-less recombination at the band edge, were explained, using tight-binding mod-

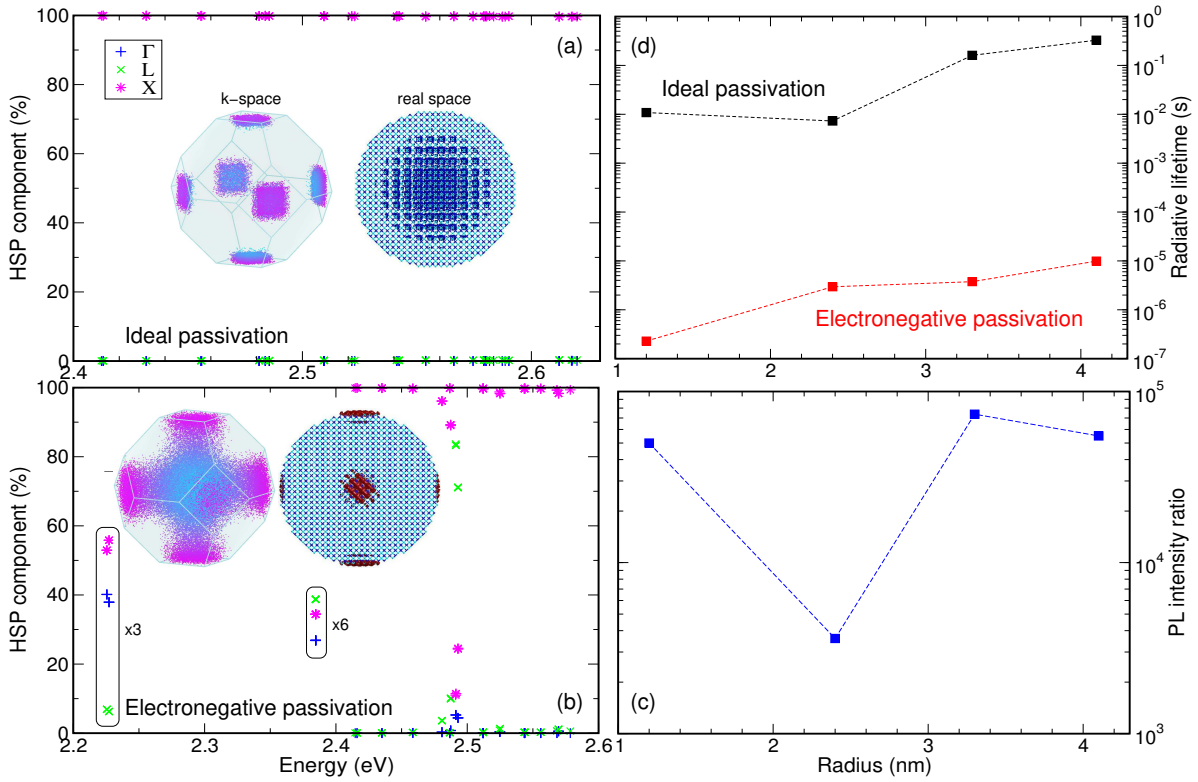

Figure 8: High symmetry points (HSP) composition [(a) and (b)] of the 60 lowermost conduction band states [Γ, blue plusses (+); X, magenta stars (*); L, green crosses (x). Each vertical set of (+,*,x) symbols corresponds to a single electronic state (which is normally 3 fold degenerate, excluding spin - indicated by "×3" in the figure; however some states are 6-fold degenerate, excluding spin - indicated by "×6"), whose energy is calculated from the VBM], calculated for AlAs NCs with $R = 4.1$ nm and either (a) ideal passivation or (b) electronegative passivation. The insets in (a) and (b) represent the CBM wave function in k-space and real space (in the former, blue dots indicate k-points close to the Γ point, whereas magenta dots indicate k-points close to X and L; in the latter, blue and cyan spheres represent Al and As atoms, respectively). (c) Ratio between the PL intensity of electronegatively passivated and ideally passivated AlAs NCs *vs* size. (d) radiative lifetimes *vs* size [ideal passivation, black symbols and line; electronegative passivation, red symbols and line].

elling, in terms of carbon's electronegativity leading to increased electron confinement at the NC surface, which resulted in a broadening of the wave function distribution in k-space - in contrast, in H-passivated NCs both electron and hole wave functions were isotropically distributed over the whole NC, yielding a bulk-like band structure.

As the electronic structure of Si and Ge NCs are homologous[33] (and the same also approximately applies to their optical properties), we would expect electronegative passivation to induce a similar behavior in the latter system. Indeed, Reboredo and Zunger,[34] showed theoretically that it is possible to modify the exciton radiative lifetime in Ge NCs by changing the electronegativity of their passivants. This leads to a change in the orbital symmetry of the VBM and to a change in the Bloch-function composition in reciprocal space (albeit from X to L - and not to Γ), of the CBM wave function.

The profound influence of the passivants' electronegativity on the optical properties of group IV NCs has therefore been extensively documented. Our study shows its universal applicability to any indirect band gap semiconductor and clarifies its origins.

A natural question to ask at this point is to what extent our passivants realistically simulate the effects of actual ligands. As explained in the Method section below (and more in detail in the Supporting Information), we passivate the unsaturated bonds at the NC surface with pseudo-hydrogenic, short-range potentials with Gaussian form.[35] The primary aim of this procedure is to remove any state from the gap (an example of the difference between core states and gap states in GaP NCs with a P-rich surface is presented in Fig. S2, Supporting Information), as would be achieved in the presence of real passivants (from this point of view, we achieve an ideal passivation). Also, the same model passivants are used for any NC size of the same material, as it would be the case with specific capping groups in experimental conditions. Apart from their effect on the surface states, however, our model ideal passivants are not conceived to simulate any specific capping groups, as the pseudo-hydrogenic potential we use is clearly an oversimplified model for a complex organic molecule. Nevertheless, our calculated ionization energies and

electron affinities have been shown to accurately reproduce the experimentally measured ones for a wide range of NCs sizes and for different materials,[37] as have our calculated optical properties.[36,38–41] Therefore we do not expect our ideal passivants to have introduced any artifacts in the calculated electronic structure of GaP. Should that have been the case (which we cannot completely rule out), and should our anion passivants be unusually electronegative, our main conclusions on how a strongly electronegative passivant can turn any indirect bandgap material into a direct one still stand, as the case of AlAs clearly proves. Indeed, in order to create electronegative passivants for AlAs NCs, it was sufficient to move the (negative) passivation potential of an ideal passivant (which reproduces the expected indirect band gap characteristics), closer to the surface anion with two dangling bonds, achieving a stronger repulsion (*i.e.*, a stronger confinement) for the hole and a stronger attraction for the electron, which localizes closer to the surface. This alteration alone led, *inter alia*, to an over-4-orders-of-magnitude increase in both radiative recombination rates and PL intensity in most of the AlAs NCs considered here.

Now the question is whether this passivant's electronegativity is unrealistic and whether it can be obtained with a real capping group. We addressed this issue in the past,[42] showing that, our pseudo-hydrogenic potential is sufficiently detailed to capture the essential properties of the capping agent's most important component - its binding moiety - which is responsible for its electronegativity.

A way to experimentally characterize this property is to measure the ionization energy shift a passivant induces in a NC (the ionization energy, IE, is defined as $IE = E_{\text{vacuum}} - E_{\text{vbm}}$). Indeed, the observed shifts in the VBM energy of InAs NCs terminated by different ligands (ranging from 0.2 to 0.4 eV) were recently linked[43] with the electronegativity of their binding moiety (with the more electronegative anchor group inducing the largest IE). Interestingly, it was also found[43] that the most important role in determining such a shift was played by the binding moiety itself, as the shift induced showed no correlation with the identity of the capping molecule's polar terminal group.

A similar conclusion was also reached in the case of CdSe NCs capped with different ligands,[37] where variations in surface moiety (but, importantly, not in the alkyl chain length for each of the moieties) were found to induce IE changes ranging from 0.05 eV up to 0.35 eV.

These findings confirm the suitability of our simplified ligand model for the purposes here investigated: the realistic modeling of a capping group's electronegativity.

Furthermore, the IE shifts induced by our model electronegative passivants (*i.e.* the difference in the VBM energy position calculated using ideal and electronegative passivation) range from 0.36 eV for an AlAs NC with $R = 1.2$ nm, to 0.017 eV for $R = 3.3$ nm, and are therefore within the range of experimentally observed values, confirming that the electronegativity of our passivants is realistic.

Unfortunately, this is as far as our model can go in terms of its capability to link our electronegative ligands to real ligands. Since, as we mentioned above, our approach only allows us to model the properties of the ligand's binding group, any attempt to identify our electronegative ligands with a specific molecule would involve a high degree of uncertainty and arbitrariness. This task is complicated even further by the fact that colloidal AlAs NCs are not currently synthesized and therefore no information is available on which capping groups are suitable to passivate their surface. In the case of GaP, the presence of an unresolved disagreement on the reported passivation for Ga-based NCs, where the same capping groups that were used successfully by some authors,[44,45] where recently found unsuitable by others,[46] also makes any assignment difficult and questionable. Therefore, having shown that our model ligands are realistic (for the purpose of this study), we are however unable to identify them with specific capping molecules.

We want to conclude by briefly addressing the applicability of our results to real NCs in experimental conditions. Although all of our calculations are performed on ideally symmetric, spherical-like NCs, our conclusions are clearly not limited to perfect structures. Indeed, the presence of "imperfections" (such as asymmetric shapes, or small

structural distortions), that naturally occur in real samples, would represent additional perturbations, that, in the light of what we discussed above, may contribute to the Γ-X mixing in the character of the CBM, leading to a further enhancement of the zero-phonon transitions. Based on the available experimental evidence, however, these contributions are expected to be negligible in most cases.

Conclusions

In conclusion we have shown that the presence of P-rich facets on the surface of strongly confined GaP NCs with zincblende crystal structure promotes strong inter-valley mixing, resulting in a Γ-like CBM and in CB states with higher Γ and L character. This yields strong band edge transitions with small Stokes shifts and short radiative lifetimes if compared with NCs with Ga-rich surfaces. On the other hand, when the NC radius exceeds ~ 1.6 nm, weak, indirect band edge transitions and long radiative lifetimes ($> 100\mu$s) are found for all surface terminations.

A strong effect of surface P has been reported previously in InP NCs,[38] where it has been shown to induce increased overlaps of the band edge wave functions in *real space*, leading, in small NCs, to reductions in the radiative lifetimes, the Stokes shifts and the PL linewidths. In the case of small GaP NCs, however, we found that the presence of P-terminated facets also leads to increased inter-valley coupling, which mixes direct Γ-like wave function character into the indirect X-like conduction band states, leading to an enhancement of the zero-phonon transitions and, ultimately, to an indirect to direct transition. We concluded that this effect is associated with (i) a strong confinement regime, (ii) a localisation of the the electron wave function away from the NC core and close to the surface, and (iii) a ratio < 1 of the electron effective masses at Γ and at the CBM (located either at/close to X or L). As condition (iii) is satisfied by nearly all indirect band gap semiconductors, we proposed a simple, general strategy that should greatly enhance the

zero-phonon transitions, even to the point to promote an indirect-to-direct transition, in any indirect band gap material. It consists of two main ingredients: (i) nanostructuring, and (ii) the use of strongly electronegative ligands to passivate the nanostructure surface. We validated it by applying it first to GaP, then to AlAs, an indirect material with a completely different composition to GaP, obtaining an increase of over 4 orders of magnitude in both the PL intensity and the radiative rate for a wide range of sizes. These results are in striking contrast to the one order of magnitude increase in the integrated PL emission and about 2 orders of magnitude decrease in the PL lifetime reported for wurtzite GaP nanowires (compared with those of a zincblende (001) bulk GaP reference sample), and adduced as evidence of a direct band gap in those nanostructures. Finally, we discussed the suitability of our model ligands for the realistic modeling of a capping group's electronegativity and the applicability of our conclusions to real NCs of any indirect bandgap material, providing ample theoretical and experimental evidence supporting both.

Method

Our NCs are built atomistically, from a central anion up to the desired radius, and, according to the findings of recent DFT calculations,[24] have the crystal structure of the bulk material. The unsaturated bonds at the surface are passivated using pseudo-hydrogenic, short-range potentials with Gaussian form,[35] which were developed in this work for GaP and AlAs (further details are provided in the Supporting Information). The single-particle energies and wave functions are obtained by solving the Schrödinger equation using the state-of-the art plane-wave semiempirical pseudopotential method (SEPM),[21] including spin-orbit coupling (here we use the pseudopotentials derived by Mattila *et al.*,[47] for GaP, and by Mäder and Zunger,[48] for AlAs). In the SEPM,[21] the single-particle Schrödinger equation, containing SEPM screened atomic potentials fitted to the DFT potentials and to the experimental band structure, is solved non-self-consistently using the folded spec-

trum method[49] for a selected set of states near the band gap. This approach allows us to obtain DFT-like accuracy in the calculation of the eigenstates of systems containing tens of thousands of atoms. Indeed SEPM and DFT bulk wave functions exhibit a 99% overlap.[21]

The k-space decomposition of the conduction band (CB) wave functions is performed following the procedure described in Ref. [41], where the high symmetry points Γ, L and X are used as seeds for a Voronoi partition of the Brillouin zone,[50,51] having the property that each wave vector contained in that partition (Voronoi cell) is closer to the specific high-symmetry point than to any other.

The optical spectra and radiative lifetimes are calculated *via* a configuration interaction scheme, including excitonic effects[52] (here we include up to 60 electron and 60 hole states - for a total of 14400 configurations - to capture the full details of the direct transition in AlAs NCs, where the Γ-like CB state is state number 57).

The thermally averaged lifetimes are calculated assuming Boltzmann occupation of higher-energy excitonic states, separated by an energy ΔE_γ, as

$$\frac{1}{\tau_R(T)} = \frac{\Sigma_\gamma (1/\tau_\gamma) e^{-\Delta E_\gamma / k_B T}}{\Sigma_\gamma e^{-\Delta E_\gamma / k_B T}} \tag{1}$$

where the radiative lifetime τ_γ for the transition from the excitonic state Ψ_γ to the ground state is obtained in the framework of time-dependent perturbation theory as

$$\frac{1}{\tau_\gamma} = \frac{4nF^2 \alpha \omega_\gamma^3}{3c^2 \left| M_\gamma \right|^2}, \tag{2}$$

α is the fine structure constant, $\hbar\omega_\gamma$ is the transition energy, c is the speed of light in vacuum, $M_\gamma = \sum_{v,c} C_{v,c}^\gamma \langle \psi_v \mid \mathbf{r} \mid \psi_c \rangle$ is the dipole matrix element of the excitonic transition, ψ_v and ψ_c are the valence (v) and conduction (c) states, solutions of the single-particle Schrödinger equation, $C_{v,c}^\gamma$ are the coefficients of the exciton wave function expansion in terms of Slater determinants,[52] n is the refractive index of the surrounding medium (here we use $n = 1.497$ for toluene, a solvent commonly used in the synthesis of NCs),

$F = 3\epsilon/(\epsilon_{dot} + 2\epsilon)$ is the screening factor, $(\epsilon = n^2)$, and ϵ_{dot} is the dielectric constant of the nanocrystal which is calculated using a modified Penn model.[52]

Supporting Information Available

The Supporting Information is available free of charge at https://pubs.acs.org
Origin of the features in the optical spectra calculated for GaP NCs with different surface stoichiometries; Passivation procedure and parameters; Surface composition of our GaP NCs; Difference between surface (gap) states and core states.

Acknowledgements

This work was undertaken on ARC3, part of the High Performance Computing facilities at the University of Leeds, UK. M.C. gratefully acknowledges financial support from the School of Electronic & Electrical Engineering, University of Leeds.

Associated Content

The authors declare no competing financial interest.

References

1. Pilkuhn, M.; Foster, L. Green Luminescence from Solution-Grown Junctions in GaP Containing Shallow Donors and Acceptors *IBM Journal of Research and Development* **1966**, *10*, 122-129.

2. Wight, D.R. Green Luminescence Efficiency in Gallium Phosphide. *J. Phys. D: Appl. Phys.* **1977**, *10* 431-454.

3. Zhang, Y.; Fluegel, B.; Mascarenhas, A.; Xin, H.P.; Tu, C.W. Optical Transitions in the Isoelectronically Doped Semiconductor GaP:N: An Evolution from Isolated Centers, Pairs, and Clusters to an Impurity Band *Phys. Rev. B* **2000**, *62*, 4493-4500.

4. Liu, C.; Sun, J.; Tang, J.; Yang, P. Zn-Doped *p*-Type Gallium Phosphide Nanowire Photocathodes from a Surfactant-Free Solution Synthesis. *Nano Lett.* **2012**, *12*, 5407-5411.

5. Tietjen, J. J.; Amick, J. A. The Preparation and Properties of Vapor-Deposited Epitaxial $GaAs_{1x}P_x$ Using Arsine and Phosphine. *J. Electrochem. Soc.* **1966**, *113*, 724-728.

6. Shan, W.; Walukiewicz, W.; Yu, K.M.; Wu, J.; Ager III, J.W. Nature of the Fundamental Band Gap in GaN_xP_{1x} Alloys. *Appl. Phys. Lett.* **2000** *76*, 3251-3253.

7. Kornienko, N.; Whitmore, D. D.; Yu, Y.; Leone, S. R.; Yang, P. Solution Phase Synthesis of Indium Gallium Phosphide Alloy Nanowires. *ACS Nano* **2015**, *9*, 3951-3960.

8. Russell, H.B.; Andriotis, A.N.; Menon, M.; Jasinski, J.B.; Martinez-Garcia, A.; Sunkara M.K. Direct Band Gap Gallium Antimony Phosphide ($GaSb_xP_{1x}$) Alloys. *Sci. Rep.* **2016**, 6, 20822.

9. Lu, X.; Huang, S. R.; Opila, R. L.; Barnett, A. Gallium Phosphide Solar Cells for Multi-Junction Systems. In *Proceedings to the 34th IEEE Photovoltaic Specialists Conference*, Philadelphia, USA, June 7-12, **2009**, 000968-000971.

10. Kotulak, N. A.; Diaz, M.; Barnett, A.; Opila, R. L. Toward a Tandem Gallium Phosphide on Silicon Solar Cell through Liquid Phase Epitaxy Growth. *Thin Solid Films* **2014**, *556*, 236-240.

11. Barton, E. E.; Rampulla, D. M.; Bocarsly, A. B. Selective Solar-Driven Reduction of CO_2 to Methanol Using a Catalyzed *p*-GaP Based Photoelectrochemical Cell. *J. Am. Chem. Soc.* **2008**, *130*, 6342-6344.

12. Malizia, M.; Seger, B.; Chorkendorff, I.; Vesborg, P. C. K. Formation of a *p-n* Heterojunction on GaP Photocathodes for H_2 Production Providing an Open Circuit Voltage of 710 mV. *J. Mater. Chem. A* **2014**, *2*, 6847-6853.

13. Murayama, M.; Nakayama, T. Chemical Trend of Band Offsets at Wurtzite/Zinc-Blende Heterocrystalline Semiconductor Interfaces, *Phys. Rev. B* **1994**, *49*, 4710-4724.

14. Yeh, C.-Y.; Wei, S.H.; Zunger, A. Relationships between the Band Gaps of the Zinc-Blende and Wurtzite Modifications of Semiconductors *Phys. Rev. B* **1994**, *50*, 2715-2718.

15. Assali, S.; Zardo, I.; Plissard, S.; Kriegner, D.; Verheijen, M. A.; Bauer, G.; Meijerink, A.; Belabbes, A.; Bechstedt, F.; Haverkort, J. E. M.; Bakkers, E. P. A. M. Direct Band Gap Wurtzite Gallium Phosphide Nanowires. *Nano Lett.* **2013**, *13*, 1559-1563.

16. Greil, J.; Assali, S.; Isono, Y.; Belabbes, A.; Bechstedt, F.; Valega Mackenzie, F. O.; Silov, A. Yu.; Bakkers, E.P.A.M.; Haverkort, J.E.M. Optical Properties of Strained Wurtzite Gallium Phosphide Nanowires. *Nano Lett.* **2016**, *16*, 3703-3709.

17. Gagliano, L.; Belabbes, A.; Albani, M.; Assali, S.; Verheijen, M.A.; Miglio, L.; Bechstedt, F.; Haverkort, J.E.M.; Bakkers, E.P.A.M. Pseudodirect to Direct Compositional Crossover in Wurtzite GaP/$In_xGa_{1-x}P$ Core-Shell Nanowires. *Nano Lett.* **2016**, *16*, 7930-7936.

18. Belabbes, A.; Bechstedt, F. Forbidden Band-Edge Excitons of Wurtzite-GaP: A Theoretical View. *Phys. Stat. Sol. B* **2019**, *256*, 1800238.

19. Kim, S.; Lee, K.; Kim, S.; Kwon, O.-Pil; Heo, J.H.; Im, S.H.; Jeong, S.; Lee, Doh C.; Kim, S.-W. Origin of Photoluminescence from Colloidal Gallium Phosphide Nanocrystals Synthesized *via* a Hot-Injection Method. *RSC Adv.*, **2015**, *5*, 2466-2469.

20. Furis, M.; Sahoo, Y.; MacRae, D.J.; Manciu, F.S.; Cartwright, A.N.; Prasad, P.N. Surfactant-Imposed Interference in the Optical Characterization of GaP Nanocrystals. *J. Phys. Chem. B* **2003**, *107*, 11622-11625.

21. Wang, L.-W.; Zunger, A. Local-Density-Derived Semiempirical Pseudopotentials. *Phys. Rev. B* **1995**, *51*, 17398-17416.

22. Mićić, O. I.; Sprague, J. R.; Curtis, C. J.; Jones, K. M.; Machol, J. L.; Nozik A. J.; Giessen H.; Fluegel, B. Mohs, G.; Peyghambarian, N. Synthesis and Characterization of InP, GaP, and $GaInP_2$ Quantum Dots. *J. Phys. Chem.* **1995**, *99*, 7754-7759

23. Zhang, Q. X.; Zhang Z. C.; Wang, B. P. Study on Optical Properties Associated with Intrinsic Defects in GaP Nanoparticles. *J. Phys. D: Appl. Phys.* **2008**, *41*, 185403.

24. Ma, X.; Min, J.; Zeng, Z.; Garoufalis, C.S.; Baskoutas, S.; Jia, Y.; Du, Z. Excitons in InP, GaP, and $Ga_xIn_{1x}P$ Quantum Dots: Insights from Time-Dependent Density Functional Theory. Phys. Rev. B **2019**, *100*, 245404.

25. Belyakov, V. A.; Burdov, V. A.; Lockwood, R.; Meldrum, A. Silicon Nanocrystals: Fundamental Theory and Implications for Stimulated Emission. *Advances in Optical Technologies* **2008**, *2008*, 279502.

26. Lee, B. G.; Luo, J.-W.; Neale, N. R.; Beard, M. C.; Hiller, D.; Zacharias, M.; Stradins, P.; Zunger, A. Quasi-Direct Optical Transitions in Silicon Nanocrystals with Intensity Exceeding the Bulk. *Nano Lett.* **2016** *16*, 1583-1589.

27. Intrinsic Properties of Group IV Elements and III-V, II-VI and I-VII Compounds. In *Landolt- Börnstein - Numerical Data and Functional Relationships in Science and Technology - Group III: Crystal and Solid State Physics*, Madelung, O.; von der Osten, W.; Rössler, U., Eds.; Springer-Verlag: Berlin Heidelberg (Germany), 1987; Vol. 22A.

28. Nakwaski, W. Effective Masses of Electrons and Heavy Holes in GaAs, InAs, AlAs and Their Ternary Compounds. *Physica B* **1995**, *210*, 1-25.

29. Ma, Y,; Pi, X.; Yang, D. Fluorine-Passivated Silicon Nanocrystals: Surface Chemistry *versus* Quantum Confinement. *J. Phys. Chem. C* **2012**, *116*, 5401-5406.

30. Lee, S.; Cho, W. J.; Han, I. K.; Choi, W. J.; Lee, J. I. White Light Emitting Silicon Nanocrystals as Nanophosphor. *Phys. Stat. Sol. b* **2004** *241*, 2767-2770.

31. Li, Q. S.; Zhang, R. Q.; Lee, S. T.; Niehaus, T. A.; Frauenheim, Th. Amine-Capped Silicon Quantum Dots. *Appl. Phys. Lett.* **2008**, *92*, 053107.

32. Dohnalová, K.; Poddubny, A. N.; Prokofiev, A. A.; de Boer, W. D. A. M.; Umesh, C. P.; Paulusse, J. M. J.; Zuilhof, H.; Gregorkiewicz, T. Surface Brightens up Si Quantum Dots: Direct Bandgap-Like Size-Tunable Emission. *Light: Sci. Appl.* **2013** *2*, e47.

33. Garoufalis, C.S. Optical Gap and Excitation Energies of Small Ge Nanocrystals. *J. Math. Chem.* **2009**, *46*, 934-941.

34. Reboredo, F. A.; Zunger, A. Surface-Passivation-Induced Optical Changes in Ge Quantum Dots. *Phys. Rev. B* **2001**, *63*, 235314-1–235314-7.

35. Graf, P.A.; Kim, K.; Jones, W.B.; Wang, L.W. Surface Passivation Optimization Using DIRECT. *J. Comput. Phys.* **2007**, *224*, 824-835.

36. Jasieniak, J.; Smith, L.; van Embden, J.; Mulvaney, P.; Califano, M. Re-Examination of the Size-Dependent Absorption Properties of CdSe Quantum Dots. *J. Phys. Chem. C* **2009**, *113*, 19468-19474.

37. Jasieniak, J.; Califano, M.; Watkins, S.E. Size-Dependent Valence and Conduction Band-Edge Energies of Semiconductor Nanocrystals. *ACS Nano* **2011**, *5*, 5888-5902.

38. Rodosthenous, P.; Gómez-Campos, F.M.; Califano, M. Tuning the Radiative Lifetime in InP Colloidal Quantum Dots by Controlling the Surface Stoichiometry. *J. Phys. Chem. Lett.* **2020**, *11*, 10124-10130.

39. Califano, M. Origins of Photoluminescence Decay Kinetics in CdTe Colloidal Quantum Dots. *ACS Nano* **2015**, *9*, 2960-2967.

40. Puangmali, T.; Califano, M.; Harrison, P. Interband and Intraband Optical Transitions in InAs Nanocrystal Quantum Dots: A Pseudopotential Approach. *Phys. Rev. B* **2008**, *78*, 245104.

41. Sills, A.; Harrison, P.; Califano, M. Exciton Dynamics in InSb Colloidal Quantum Dots. *J. Phys. Chem. Lett.* **2015** *7*, 31-35

42. Califano, M. Suppression of Auger Recombination in Nanocrystals *via* Ligand-Assisted Wave Function Engineering in Reciprocal Space. *J. Phys. Chem. Lett.* **2018**, *9*, 2098-2104.

43. Soreni-Harari, M.; Yaacobi-Gross, N.; Steiner, D.; Aharoni, A.; Banin, U.; Millo, O.; Tessler, N. Tuning Energetic Levels in Nanocrystal Quantum Dots through Surface Manipulations. *Nano Lett.* **2008**, *8*, 678-684.

44. Beberwyck, B. J.; Alivisatos, A. P. Ion Exchange Synthesis of III-V Nanocrystals *J. Am. Chem. Soc.* **2012**, *134*, 19977-19980.

45. Lauth, J.; Strupeit, T.; Kornowski, A.; Weller, H. A Transmetalation Route for Colloidal GaAs Nanocrystals and Additional III-V Semiconductor Materials *Chem. Mater.* **2013**, *25*, 1377-1383.

46. Srivastava, V.; Liu, W. Y.; Janke, E. M.; Kamysbayev, V.; Filatov, A. S.; Sun, C. J.; Lee, B.; Rajh, T.; Schaller, R. D.; Talapin, D. V. Understanding and Curing Structural Defects in Colloidal GaAs Nanocrystals. *Nano Lett.* **2017**, *17*, 2094-2101.

47. Mattila, T.; Wang, L.-W.; Zunger, A. Electronic Consequences of Lateral Composition Modulation in Semiconductor Alloys. *Phys. Rev. B* **1999**, *59*, 15270-15284.

48. Mäder, K.A.; Zunger, A. Empirical Atomic Pseudopotentials for A1As/GaAs Superlattices, Alloys, and Nanostructures. *Phys. Rev. B* **1994**, *50*, 17393-17405.

49. Wang, L.-W.; Zunger, A. Solving Schrödingers Equation around a Desired Energy: Application to Silicon Quantum Dots *J. Chem. Phys.* **1994**, *100*, 2394-2397.

50. Aurenhammer, F. Voronoi Diagrams - A Survey of a Fundamental Geometric Data Structure. *ACM Computing Surveys* **1991**, *23*, 345-405;

51. Okabe, A.; Boots, B.; Sugihara, K.; Chiu, S. N. *Spatial Tessellations - Concepts and Applications of Voronoi Diagrams*. 2nd edition. John Wiley, Chichester, 2000, ISBN 0-471-98635-6;

52. Franceschetti, A.; Fu, H.; Wang, L. W.; Zunger, A. Many-Body Pseudopotential Theory of Excitons in InP and CdSe Quantum Dots. *Phys. Rev. B* **1999**, *60*, 1819-1829.

Graphical TOC Entry